CORE
Metadata, citation and similar papers at core.ac.uk
Provided by Archivio della ricerca- Università di Roma La Sapienza

PROFESSOR ELISABETTA FERRETTI (Orcid ID : 0000-0001-7265-6429)

Article type : Original Article

The miR-139-5p regulates proliferation of supratentorial paediatric low-grade gliomas by targeting the PI3K/AKT/mTORC1 signalling

Giuseppina Catanzaro[1], Zein Mersini Besharat[2], Evelina Miele[3*], Martina Chiacchiarini[2,3], Agnese Po[2], Andrea Carai[4], Carlo Efisio Marras[4], Manila Antonelli[5], Manuela Badiali[6], Alessandro Raso[7], Samantha Mascelli[7], Daniel Schrimpf [8,9], Damian Stichel[9], Marco Tartaglia[10], David Capper[8,9,11], Andreas von Deimling[8,9], Felice Giangaspero[5,12,#], Angela Mastronuzzi[13], Franco Locatelli[13,14], Elisabetta Ferretti [1,12,#]

[1]Department of Experimental Medicine, Sapienza University, Rome

[2]Department of Molecular Medicine, Sapienza University, Rome

[3]Center for Life NanoScience@Sapienza, IIT, Rome (M.C.)

[4]Department of Neuroscience and Neurorehabilitation, Neurosurgery Unit, Bambino Gesù Children's Hospital, IRCCS, Rome

[5]Department of Radiological, Oncological and Pathological Science, Sapienza University, Rome

[6]Bone Marrow Transplantation Unit, Microcitemico Children's Hospital, Cagliari

[7]Giannina Gaslini Institute, Genoa

[8]Department of Neuropathology, Heidelberg University (A.v.D., D.S., D.C)

[9]German Cancer Research Center (DKFZ) and German Cancer Consortium (DKTK), Clinical Cooperation Unit (CCU) Neuropathology, Heidelberg (A.v.D., D.S., D.C)

[10]Genetics and Rare Diseases Research Division, Bambino Gesù Children's Hospital, Rome

[11]Department of Neuropathology, Charité Universitätsmedizin Berlin, (D.C.)

[12]IRCCS Neuromed, Pozzilli, Isernia (F.G., E.F.)

[13]Department of Hematology/Oncology and Stem Cell Transplantation, Bambino Gesù Children's Hospital, IRCCS, Rome

[14]University of Pavia, Pavia (F.L.)

[*]Current address: Department of Hematology/Oncology and Stem Cell Transplantation, Bambino Gesù Children's Hospital, IRCCS, Rome

This article has been accepted for publication and undergone full peer review but has not been through the copyediting, typesetting, pagination and proofreading process, which may lead to differences between this version and the Version of Record. Please cite this article as doi: 10.1111/nan.12479

This article is protected by copyright. All rights reserved.

Accepted Article

Accepted Article

[#]Corresponding authors:

Elisabetta Ferretti; E-mail elisabetta.ferretti@uniroma1.it; Viale Regina Elena, 291, 00161, Rome, Italy; Phone number: +39 0649255135; Fax number: +39 0649255660;

Felice Giangaspero: E-mail felice.giangaspero@uniroma1.it; Viale Regina Elena, 291, 00161, Rome, Italy; Phone number: +39 0649979175; Fax number: +390649979175

Keywords

Paediatric low-grade gliomas; supratentorial; microRNAs; miR-139-5p; patients' derived primary cells; PI3K/AKT/mTORC1

Running Title: MiR-139-5p regulates PI3K/AKT/mTORC1 in pLGGs

Abstract

Aims: Paediatric low-grade gliomas (pLGGs) are a heterogeneous group of brain tumours associated with a high overall survival: however, they are prone to recur and supratentorial lesions are difficult to resect, being associated with high percentage of disease recurrence. Our aim was to shed light on the biology of pLGGs.

Methods: We performed microRNA profiling on 45 fresh-frozen grade I tumour samples of various histological classes, resected from patients aged ≤ 16 years. We identified 93 microRNAs specifically dysregulated in tumours as compared to non-neoplastic brain tissue. Pathway analysis of the microRNAs signature revealed PI3K/AKT signalling as one of the centrally enriched oncogenic signalling. To date, activation of the PI3K/AKT pathway in pLGGs has been reported, although activation mechanisms have not been fully investigated yet.

Results: One of the most markedly down-regulated microRNAs in our supratentorial pLGGs cohort was miR-139-5p, whose targets include the gene encoding the PI3K's (phosphatidylinositol 3-kinase) catalytic unit, *PIK3CA.* We investigated the role of miR-139-5p in regulating PI3K/AKT signalling by the use of human cell cultures derived from supratentorial pLGGs. MiR-139-5p overexpression inhibited pLGG cell proliferation and decreased the phosphorylation of PI3K target AKT and p70 S6K, a hallmark of PI3K/AKT/mTORC1 signalling activation. The effect of miR-139-5p was mediated by PI3K inhibition, as suggested by the decrease in proliferation and phosphorylation of AKT and p70 S6K after treatment with the direct PI3K inhibitor LY294002.

This article is protected by copyright. All rights reserved.

Accepted Article

Conclusions: These findings provide the first evidence that down-regulation of miR-139-5p in supratentorial pLGG drives cell proliferation by de-repressing PI3K/AKT signalling.

List of Abbreviations

Paediatric low-grade gliomas, pLGGs; Phosphatidylinositol 3-kinase, PI3K; Low-grade gliomas, LGGs; World Health Organization, WHO; Central Nervous System, CNS; Pilocytic Astrocytomas, PAs; oncogene-induced senescence, OIS; Gangliogliomas, GGs; Dysembryoplastic Neuroepithelial Tumours, DNETs; Angiocentric Gliomas, AGs; Paediatric high-grade gliomas, pHGGs; Quantitative PCR, qPCR; Formalin-fixed paraffin-embedded, FFPE; haematoxylin and eosin, H&E; Real-Time quantitative PCR, RT-qPCR; Taqman Low Density Array, TLDA; Hank's Balanced Salt Solution, HBSS; Senescence-Associated-β-galactosidase, SA-β-gal; t-Distributed Stochastic Neighbor Embedding, TSNE; Paraformaldehyde, PFA; Room Temperature, RT; Donkey Serum, DS; Phosphate Buffered Saline, PBS; Glial-Fibrillary Acidic Protein, GFAP; Glioneuronal Tumour, GNT; Controls, CTRL; Phosphorylated AKT, p-AKT; Mammalian Target of Rapamycin complex 1, mTORC1; Phosphorylated p70 S6K, p-p70 S6K; Phosphatase and tensin homolog, PTEN; Phosphoinositide-dependent kinase 1, PDK-1; Tuberous sclerosis complex 2, TSC2; Ras homolog enriched in brain, Rheb.

Introduction

The most commonly diagnosed brain tumours in children are low-grade gliomas (LGGs). Paediatric LGGs (pLGGs) include different entities, as defined by the revised World Health Organization (WHO) Classification of Central Nervous System (CNS) Tumours, which is based on both histological and molecular features [1]. The vast majority of pLGGs are pilocytic astrocytomas (PAs), and they are the ones that have been studied most thoroughly. These tumours are driven by dysregulated signalling through the MAPK/ERK pathway [2]. Less is known about the biological characteristics of less common pLGGs which include, among others, gangliogliomas (GGs), dysembryoplastic neuroepithelial tumours (DNETs), and angiocentric gliomas (AGs).

The location of pLGGs has a major impact on outcome since it determines the tumour's resectability. Infratentorial pLGGs, which occur mainly in the cerebellum, can often be cured by surgery. Supratentorial tumours and those arising in the brainstem are much more difficult to resect, and residual or recurrent disease is, therefore, a common event. The latter are treated with radiotherapy or conventional chemotherapy (e.g. SIOP-LGG 2004 protocol). However, both treatments are associated with substantial long-term toxicity, and these tumours frequently evolve into chronic disease with high morbidity [2-6].

The genomic landscape of pLGGs is now being defined. The most frequent genetic alterations are the *KIAA1549-BRAF* fusion gene and the BRAF V600E single point mutation [3]. Other mutations, such as *FGFR1* alterations, are mainly expressed only by specific pLGGs subtypes, such as DNET [7]. Along with the dysregulated MAPK/ERK signalling mentioned above [8-10], aberrant activation of the PI3K/AKT signalling pathway, which can be demonstrated by high levels of phosphorylated AKT, is also a well-documented feature of gliomas, including pLGGs [3, 11, 12]. In

This article is protected by copyright. All rights reserved.

Accepted Article

some cases, its dysregulation has been linked to genetic changes, such as *BRAF* fusions, *FGFR1* duplications and *MYB* rearrangements [3], or epigenetic modifications, but in many cases the mechanism underlying PI3K/AKT pathway activation is still unknown.

MicroRNAs are emerging as major regulators of cancer-related gene expression. In this study, we examined the role of dysregulated microRNA expression in pLGGs, in particular in pLGGs arising in supratentorial areas of the brain, which have the poorest clinical outcomes. Our microRNA profiling analysis of a large series of grade I LGGs from paediatric patients pointed to the PI3K/AKT pathway as one of the most likely "targets" of dysregulated microRNA expression. In particular, we identified a novel microRNA-mediated mechanism that could be responsible for the hyper-activation of the PI3K/AKT signalling pathway. It involves the markedly down-regulated expression of miR-139-5p, which was observed in the pLGG samples we analysed. Dysregulation of miR-139-5p has been linked to various types of cancer, including adult gliomas and paediatric high-grade gliomas (pHGGs) [13-15], but its role in pLGGs has *not* been investigated yet. Our functional studies in short-term cultures from primary supratentorial pLGGs indicate that the down-regulation of miR-139-5p in these tumours promotes PI3K/AKT pathway activation, thereby enhancing pLGG cell growth.

Materials and Methods

Unless otherwise stated, commercially available products were used according to the manufacturer's instructions / protocols.

Tumour samples and controls

MicroRNA profiling was performed with quantitative PCR (qPCR) (as described below) on RNA extracted from snap-frozen tumour tissue samples from 45 patients (aged 1–16 years) with pLGGs. All underwent surgery at the Bambino Gesù Children's Hospital in Rome or the Gaslini Institute in Genoa between 2014 and 2016. The clinical and pathological features of each case are summarized in Table 1.

RNA and DNA used for the analyses were extracted from tumour samples with pathologist-confirmed tumour cell contents of 80% or more. For control purposes, we profiled eight samples (three + a pool of five) of non-neoplastic brain tissue purchased from Ambion-Life Technology (Thermo Scientific, Wilmington, MA, USA) (*n*=1: AM7962, Human Brain Total RNA) or Biochain Institute (Newark, CA, USA) (*n*=7: R1234035-50, Total RNA-Human Adult Normal Tissue-Brain; R1234035-P, Total RNA-Human Adult Normal Tissue-5 Donor Pool-Brain; R1234035-50, Total RNA-Human Adult Normal Tissue-Brain) and 28 samples (four + a pool of 24) of non-neoplastic brain cerebellum purchased from Biochain Institute (*n*=4: R1234039-50, Total RNA-Human Brain cerebellum) or Clontech Laboratories (Takara Bio USA Inc., Shiga, Japan) (*n*=1: 636535, Total RNA-Human Brain cerebellum-24 Donor Pool-Brain). MicroRNA profiles for the pLGGs were also compared with profiles previously reported by our group for 13 pHGGs, which had been collected between 2005 and 2010 from patients aged from 3 to 17 years [15]. To ensure the comparability of these two cohorts, we re-analysed the microRNA profiles originally reported for the pHGGs [15]

This article is protected by copyright. All rights reserved.

using the same normalization procedure and statistical methods employed for comparing the pLGGs with healthy brain tissues, as reported below.

For functional studies, we established short-term cultures of pLGG cells isolated from four primary tumours resected at Bambino Gesù Children's Hospital (Rome) in 2016 (Table 2). We deliberately selected tumours with non-PA histology, since the biology of these pLGGs has been much less thoroughly explored than that of PAs. We also limited our analysis to supratentorial pLGGs, which are associated with lower miR-139-5p levels, lower resectability rates and worse outcomes than their infratentorial counterparts [11].

Histology

Formalin-fixed paraffin-embedded (FFPE) samples of each of the 45 pLGGs used in the study were sectioned (3-µm) and stained with haematoxylin and eosin (H&E) for histology. All tumour diagnoses were then confirmed by consensus decision of 3 neuropathologists (F.G., M.A., and F.D.C.) using the WHO classification criteria [1].

Immunohistochemistry

Immunohistochemical studies were performed using anti-PIK3CA (Clinisciences, Nanterre, France), anti-phospho-p70 S6 kinase (Thr389) and anti-phospho-Akt (Ser473) (Cell Signalling Technology, Danvers, MA, USA). Paraffin-embedded slices of supratentorial pLGG tissues derived from the Pathology Department of the Bambino Gesù Children's Hospital in Rome were used for the staining.

For validation of PIK3CA, phospho-p70 S6 kinase (p-p70 S6K) and phospho-AKT (p-AKT) immunohistochemical assay we tested positive tissues. Hepatocellular carcinoma samples were used for PIK3CA and breast cancer samples were used for p-p70 S6K and p-AKT. For negative control primary antibody was omitted. For the evaluation of PIK3CA, p-p70 S6K and p-AKT staining we used a scoring system. We considered: 0 for no staining; 1+ for barely perceptible staining; 2+ for light to moderate staining; and 3+ for moderate to heavy staining.

RNA extraction of pLGG tissues and cells

Please see Supplementary Materials and Methods for a detailed description.

Analysis of *BRAF* status

Each of the 45 pLGGs and the four patient-derived pLGG cell lines were analysed for the two most common genetic alterations found in these tumours—namely, the BRAF V600E point mutation (V600E) and the *KIAA1549:BRAF* fusion gene (including the three most frequent variants: *KIAA1549-BRAF* exon 16-exon 9 [K16B9], KIAA1549-BRAF exon 16-exon 11 [K16B11], and *KIAA1549-BRAF* exon 15-exon 9 [K15B9]).

This article is protected by copyright. All rights reserved.

Accepted Article

Accepted Article

BRAF fusion analysis was performed on tumour cDNAs with the Applied Biosystems Viia7 Real-Time quantitative PCR (RT-qPCR) System, as described by Tian *et al.* [16] and validated by PCR-based Sanger sequencing through amplification with specific pairs of primers flanking the fusion point between the *KIAA1549* (in exon 15 or 16) and *BRAF* (in exon 9 or 11) genes, as described by Jones *et al.* [17]. The purified PCR products were sequenced on an ABI 3130 XL DNA analyzer (Applied Biosystems) using the BigDye Terminator v1.1 Cycle Sequencing Kit (Applied Biosystems) and the forward or reverse primer used to perform the PCR. The primer sequences were as follows: *KIAA1549* exon 15: 5′-CGG AAA CAC CAG GTC AAC GG-3′; *KIAA1549* exon 16: 5′-AAA CAG CAC CCC TTC CCA GG-3′; *BRAF* exon 9: 5′-CTC CAT CAC CAC GAA ATC CTT G-3′; *BRAF* exon 11: 5′-GTT CCA AAT GAT CCA GAT CCA TTC-3′.

BRAF V600E mutation. DNA was extracted from fresh-frozen samples and patient-derived pLGG cell lines using the QIamp DNA Mini kit (Qiagen Inc., CA, USA). Quantity and quality were evaluated with a Nanodrop ND-1000 spectrophotometer (Thermo Scientific). RT-qPCR was performed, as described by Diniz et al. [18], using TaqMan probes (Life Technologies): BRAF_476_mu, which detects T>A transversion at position c.1799, and the reference-gene probe BRAF_rf. Threshold cycle (Ct) values were analysed using Mutation Detector™ Software (Life Technologies). Genomic DNA extracted from BRAF V600E and BRAF wild-type colon cancer cell lines, kindly provided by Prof. Matilde Todaro (University of Palermo), were used as positive and negative controls, respectively.

MicroRNA profiling and data analysis

MicroRNA expression profiling was performed on the pLGG tumours using RT-qPCR with Taqman Low Density Array (TLDA) microfluidic cards (Human miR v3.0, Applied Biosystems), which detect the 754 best characterized members of the human microRNA genome. Each reverse transcriptase reaction was performed with specific primers according to Applied Biosystems protocols. The same method had been used to profile the pHGGs in [15].

Statistical analysis was performed with StatMiner™ software, v. 5.0 (Integromics TM). MicroRNA expression levels were normalized by using the global expression normalization method and the comparative threshold cycle method was used to calculate the relative microRNA expression. MicroRNAs with Ct values > 33 were excluded. Differential expression between groups was assessed with the Limma test, and p values < 0.05 were considered to be statistically significant.

A single-assay qPCR for assessment of miR-139-5p expression (Code:002289) was carried out in triplicate using the TaqMan Individual microRNA assays (Applied Biosystems), as previously described [15]. Information regarding microRNA clusters was obtained from miRBase v.21 (http://www.mirbase.org/) [19]. Validated targets of hsa-miR-139-5p were identified by interrogation of the miRTarBase (http://mirtarbase.mbc.nctu.edu.tw/; [20]) and literature reports [13, 14].

This article is protected by copyright. All rights reserved.

Accepted Article

MicroRNAs clustering analysis

Dendrograms and heat maps were generated with the use of R (http://www.r-project.org/) using differentially expressed microRNAs as input. The Bray-Curtis method and the average linkage were used in hclust to cluster the samples and heatmap.2 to generate the heat maps [21].

DIANA mirPath analysis

The microRNAs that were differentially expressed in pLGGs (vs. non-neoplastic brain tissue controls) were loaded into the DIANA mirPath tool (http://snf-515788.vm.okeanos.grnet.gr/) [22] for microRNA pathway analysis. MicroRNAs that were significantly dysregulated in the tumours were then analysed to identify their putative targets.

Patient-derived primary pLGG cell cultures

Culture and characterization. Human pLGG samples (described above) were collected immediately after resection and placed in Hank's Balanced Salt Solution (HBSS) supplemented with 0.5% glucose and penicillin-streptomycin. The tissues were triturated with a serological pipette. DNAse I was added (final concentration 0.04%) and left for 20 min. Cell aggregates were then mechanically disrupted with pipettes of decreasing bore size. The single-cell suspension thus obtained was then centrifuged, and the cells suspended in NHA complete medium (Lonza, Basel, CH), counted and plated at a density of 160,000/mL. Prior to use in experiments, isolated primary pLGG cells underwent quality control assays to ensure they were reliable pLGG models. To this end, we verified that the *BRAF* status of each cell line was identical to that of the parent tumour (as described above in Analysis of *BRAF* status). For the three primary pLGG cells whose primary tumour did not show any genetic alteration on the BRAF gene, we compared methylation profiles to verify similarity between the primary cell line and the parental tumour. Immunofluorescence staining (described below) was used to confirm that the cells' histotype-specific glial / neuronal cell biomarker profile was consistent with those described in the literature [23-25]. The percentage of senescent cells was also evaluated by staining for Senescence-Associated-β-galactosidase (SA-β-gal, described below). Cultures with SA-β-gal-positivity rates of 60% or more were excluded from experimentation. During the study, cells were discarded after a maximum of 8 passages (about 30 days of culture) or when SA-β-gal-positivity rates reached 60%.

Cell treatments. Synthetic miR-139-5p (miRIDIAN microRNA code: C-310568-07, Dharmacon) or negative control (miRIDIAN microRNA negative control code: CN-001000-01, Dharmacon) were transfected into pLGG primary cells at 20 nM using HiPerFect transfection reagent (Qiagen Inc., CA, USA) for 48 h. miR-139-5p overexpression was confirmed by single assay qRT-PCR. For pharmacological inhibition of PI3K, LY294002 was purchased from Sellekchem, dissolved in DMSO, and stored until used in aliquots at -80°C as 50 mM stock solutions. LY294002 and CTRL (0.1% DMSO) were diluted in culture medium just before use. After 30 min of treatment with 50 µM LY294002, cells were shifted in normal culture medium for a recovery period of 48 h.

This article is protected by copyright. All rights reserved.

Accepted Article

Cell growth was evaluated after 48 h by trypan blue exclusion assay. Specifically, the number of cells that did not take up trypan blue (viable cells) was counted both after transfection of synthetic miR-139-5p or negative control. The number of cells that took up trypan blue (non-viable cells) was counted. Each sample was measured in triplicate and repeated at least three times.

DNA Methylation Array Data Generation

DNA methylation profiling using the Illumina Infinium HumanMethylation EPIC BeadChip array was performed according to the manufacturer's instructions at the Genetics and Rare Diseases Research Division, Bambino Gesù Children's Hospital, Rome, Italy. In detail 250 ng of DNA was used as input material for fresh-frozen tissue and primary cell line samples (after about 15 days of culture). t-Distributed Stochastic Neighbor Embedding (TSNE) analysis was conducted as previously described [26]. Basic array processing and clustering analysis were performed using Illumina GenomeStudio V2011.1 (Methylation Module version 1.9.0, content descriptor version 1.2). (https://www.illumina.com/techniques/microarrays/array-data-analysis-experimental-design/genomestudio.html) (Illumina, Inc., San Diego, CA). Signal intensities were obtained without background subtraction and normalized to internal controls. Beta-values were used for downstream methylation analyses.

Immunofluorescence studies

Please see Supplementary Materials and Methods for a detailed description.

Senescence-Associated-β-galactosidase activity

SA-β-gal activity was assessed as described in Debacq-Chainiaux [28] with minor modifications. Briefly, cells were fixed with 3.6% of formaldehyde in PBS for 4 min at RT. Fixed cells were washed and incubated overnight with freshly prepared staining solution at 37°C in the absence of CO_2. The cells were washed, and coverslips were mounted in antifade medium (Dako Fluorescence mounting medium, Agilent Technologies, Santa Clara, CA). Images were acquired using a Leica DM2500 microscope (Leica Microsystems, Wetzlar, Germany) with a 20x/0.40 NA objective. Pictures were taken using the ISCapture software and processed with Adobe Photoshop (Mountain View, CA) to adjust brightness and contrast. The percentage of positive cells was evaluated by dividing the number of blue cells on the total number of cells in the field [8].

Western Blotting

Please see Supplementary Materials and Methods for a detailed description.

This article is protected by copyright. All rights reserved.

Accepted Article

Statistical Analysis

Data reported in this paper are the means ± SD of at least three independent experiments each performed in triplicate. Unpaired t-test and Paired t-test were performed wherever appropriate using GraphPad Prism Software version 6.0 (CA, USA), p values < 0.05 were considered to be statistically significant.

Results

Characteristics of the pLGG cohort

The clinical and pathological features of the 45 primary pLGGs we analysed are summarized in Table 1. Thirty (67%) of the tumours were pilocytic astrocytomas (PAs), eight (18%) were gangliogliomas (GGs), four (9%) were dysembryoplastic neuroepithelial tumours (DNETs), two (4%) were angiocentric gliomas (AGs), and one (2%) was a glioneuronal tumour (GNT). Patients' age at diagnosis ranged from 1 to 16 years (median 7 years; mean 7.1 years). Three were located in the brain stem (two PAs, one GG). The other 42 included comparable numbers of infratentorial (n=25) and supratentorial (n=17) tumours. *KIAA1549:BRAF* fusion genes were common, in accordance to literature [3]. The K16B9 variant—the one most frequently encountered—was present in 18 (27%) pLGGs, most of which (13, 52%) were infratentorial. *BRAF* fusions were less common in the supratentorial tumours (5/18 [29%]). Three pLGGs harboured the BRAF V600E point mutation (two infratentorial and one supratentorial).

MicroRNA profiles of pLGGs

We measured the expression levels of 754 microRNAs in the 45 pLGGs described above and compared them with non-neoplastic brain (controls, CTRL). The results were also compared with profiles previously reported by our group for 13 pHGGs (glioblastoma multiforme, *n*=8; anaplastic astrocytoma, *n*=5) [15]. The TaqMan Low Density Array (TLDA) analysis reported similar high detection rates in all the three tissue groups (474 [63%] of the 754 microRNAs were identified in pLGGs, 436 [58%] in pHGGs, and 368 [49%] in controls).

The differentially expressed microRNAs (Supplementary Tables 1 and 2) were plotted using hierarchical clustering, as reported in Fig.1. Some of the most striking alterations involved upregulation of microRNAs with documented oncogenic effects in many tumours (e.g., miR-21 and members of the miR-17-92 cluster [15, 30]) or down-regulation of microRNAs with reported oncosuppressive effects in various settings. The latter included miR-218 [31], miR-124 [30], miR-487b [32], and miR-139-5p [33-37].

We further evaluated the microRNAs profiles of supratentorial and infratentorial tumours with respect to non-neoplastic brain or normal cerebellum as controls (CTRL), respectively. Among supratentorial tumours, 69 microRNAs displayed significant tumour-related upregulation (n=28) or down-regulation (n=41) ($p < 0.05$) (Tables 3 and 4). Whereas in the analysis between infratentorial

This article is protected by copyright. All rights reserved.

Accepted Article

tumours and normal cerebellum 109 microRNAs displayed significant tumour-related up (n=52) or down-regulation (n=57) ($p < 0.05$) (Supplementary Tables 3 and 4).

Among dysregulated microRNAs, miR-139-5p was noteworthy since it was significantly down-regulated only in supratentorial pLGGs (Table 4) and its down-regulated expression has been documented in high-grade gliomas (adult and paediatric) [13-15], but still unexplored in pLGGs.

Interestingly, the number of differentially expressed microRNAs in pLGGs and pHGGs was lower than that observed when pLGGs were compared with non-neoplastic brain tissues (Supplementary Tables 5 and 6). The pLGG and pHGG samples segregated into two main clusters (Supplementary Fig. 1). The first (left side of Supplementary Fig. 1) comprised 19 of the 45 pLGGs. The second (right side of Supplementary Fig. 1) was more heterogeneous and contained two sub-clusters: one contained 21 pLGGs, the second included both pLGGs and pHGGs. This finding highlighted the existence of a gradient of microRNA expression reflecting internal variation within the pLGGs cohort. Notably, the expression levels of miR-139-5p in pLGGs resembled those found in pHGGs.

PI3K/AKT signalling is controlled by microRNAs that are dysregulated in pLGGs

To explore the functional implications of the microRNA profile of our pLGGs cohort, we used the DIANA miRPath tool to identify signalling pathways likely to be vulnerable to the altered microRNA expression levels found in these tumours. As summarized in Table 5**,** after the broader category pathways in cancer, the PI3K/AKT pathway contained the highest number of components putatively targeted by the microRNAs dysregulated in our pLGG cohort. This finding is consistent with recent reports of aberrant PI3K/AKT/mTOR signalling in paediatric gliomas, both high- and low-grade [11, 12]. This hyper-activation has been attributed to genetic and epigenetic alterations in certain glioma subsets, but in many cases the cause is still unknown. We noted with interest, therefore, that *PIK3CA,* which encodes the catalytic subunit of phosphatidylinositol 3–kinase (PI3K), is a validated target of miR-139-5p, as demonstrated by luciferase assay in Krishnan *et al.* [38]. The marked dysregulation of this tumour-suppressor microRNA in pLGGs was documented for the first time in our cohort (Supplementary Table 2 and Table 4).

Downregulation of miR-139-5p in pLGGs favours tumour-cell proliferation

Taken together, these findings suggested that down-regulation of miR-139-5p in supratentorial tumours might contribute to the development of pLGGs by de-repressing expression of PIK3CA*,* thereby favouring aberrant activation of the PI3K/AKT pathway. To address this hypothesis, we firstly investigated the expression of PIK3CA by performing immunohistochemistry assay in pLGG tissues derived from AG, DNET and GG tumours, which are predominantly supratentorial. As reported in Supplementary Figure 2, pLGGs showed positive staining for PIK3CA, with an average of 25% positive cells and a 2 +/3 + score. Then, we carried out *in vitro* experiments in primary monolayer cultures of pLGG cells isolated from patient-derived samples of AG, DNET, and GG. The characteristics of these cells are summarized in Table 2 and their growth curves and description are reported in greater detail in Figures 2 and 3 and Supplementary Figs. 3 and 4. The

This article is protected by copyright. All rights reserved.

Accepted Article

immunofluorescence staining confirmed the glial and/or mixed neuro-glial nature of the primary pLGG cells. For all the histological types, cells were positive for the glial markers vimentin and S100, while the level of GFAP positivity was more variable ranging from 20 to 70%. In DNET and GG samples, we also detected frequent positivity for NeuN and Synaptophysin, neuronal markers, which conversely were absent in the AG. Therefore, the immunofluorescence staining together with the methylation profiling, a method to evaluate the similarity among tumours samples and their derived primary cells [10, 26, 39-41], indicate that our primary cells are a suitable and trustworthy model to study supratentorial pLGGs biology.

MiR-139-5p levels in supratentorial pLGGs were markedly lower than those in non-neoplastic total brain tissues (Table 4, Fig. 4a). Downregulation of miR-139-5p was also evident in our patient-derived primary pLGG cell cultures at levels comparable to those of the primary tumours they derive from (Fig. 4b). Overexpression of miR-139-5p in these cells (Supplementary Fig. 5) resulted in significantly reduced proliferation, which was evident in all three histological types represented (Fig. 4c-f), while not affecting cell death (Data not shown).

miR-139-5p controls PI3K/AKT/mTORC1 signalling in supratentorial pLGGs

The results of the previous experiments provide evidence that down-regulation of miR-139-5p plays a role in supratentorial pLGG cell growth. To determine whether its effects on cell growth were mediated by de-repressed PI3K activity, we assessed the effects of miR-139-5p overexpression on the phosphorylation of the PI3K target, AKT. At baseline, phosphorylated AKT (p-AKT) levels were high in all the cell cultures tested, but they dropped markedly after miR-139-5p overexpression (Fig. 5a-c). In order to investigate whether miR-139-5p effect was directly mediated by PI3K inhibition, we examined proliferation and p-AKT levels in primary pLGG cells before and after treatment with the direct PI3K inhibitor LY294002. Our results showed that LY294002 treatment caused a significant impairment of cell proliferation (Fig. 5d-g) and decreased levels of phosphorylated AKT (p-AKT) (Fig.5h-j). Again, we did not observe any significant effect on cell death (Data not shown).

One of the downstream effectors of PI3K/AKT signalling is mammalian target of rapamycin complex 1 (mTORC1). Activation of this complex has already been reported in pLGGs [11], and hyper-activation of the PI3K/AKT/mTORC1 axis has been implicated in the increased cell proliferation of these tumours [12]. We therefore wondered if mTORC1 inhibition was involved in the anti-proliferative effects produced in pLGG cells by miR-139-5p overexpression. As shown in Figure 6a-c, cells transfected with miR-139-5p displayed significantly decreased phosphorylation of p70 S6K (p-p70 S6K), a hallmark of mTORC1 activation. A comparable reduction was produced when PI3K was inhibited with LY294002 (Fig. 6d-f). Furthermore, immunohistochemical staining for p-p70 S6K and p-AKT were performed in pLGG samples. As reported in Supplementary Figures 6 and 7, tumours showed p-p70 S6K and p-AKT positive staining with an average of more than 10% positive cells and a score 2+ for both assay. Taken together, these data indicate that the down-regulated expression of miR-139-5p in primary supratentorial pLGG cells increases their proliferation by de-repressing PI3K/AKT signalling and that its effect is mediated by mTORC1, as summarized in Figure 7.

This article is protected by copyright. All rights reserved.

Accepted Article

Discussion

MicroRNAs have been identified as pivotal players in a variety of cancers [42, 43]. Thus far, however, the research conducted on these noncoding RNA species in pLGGs has been largely descriptive. Moreover, the conclusions that can be drawn from these studies are frequently limited by the small number of cases analysed [31, 44], the inclusion of high-grade gliomas besides pLGGs [45, 46] or the inclusion of adult patients [32].

Our study differs from its predecessors in several respects. Our microRNA profiling study was conducted on fresh-frozen samples of 45 pLGGs, all of which were grade I tumours resected from patients 16 years of age or younger. We identified 93 microRNAs whose differential expression distinguished the pLGGs from controls. Since a number of microRNAs display directional and quantitative similar dysregulation in pHGG, these microRNAs are more likely to play a role in paediatric gliomas in general than in specific WHO classes of pLGGs. In fact, the down-regulated expression of miR-487b, miR-323a-3p, and miR-410—all members of the 379-656 cluster—has already been described in gliomas of various grades [32, 47, 48]. Likewise, upregulated expression of miR-18a-5p and miR-20a-5p (both belonging to the miR 17-92 cluster) and of miR-21-5p has been found in pLGGs [32] and pHGGs [15, 49, 50], as well as in other types of brain tumours [51-53]. Thanks to the results of this first part of the study we were able to identify specific microRNA profiles for pLGGs that will be object of future experimental investigations.

The importance of the PI3K/AKT/mTOR pathway that emerged from our microRNA pathway analysis was not surprising. Along with the MAPK/ERK axis, it is one of the pathways most frequently upregulated in cancers, including pLGGs [2, 3, 54, 55]. Aberrant activation of PI3K/AKT/mTOR signalling in pLGGs has been reported in association with several genetic alterations, including *BRAF* fusions, *FGFR1* duplications, and *MYB* rearrangements [3], which are present at different frequencies in the various pLGGs histologies, with the last two genetic alterations that have been more specifically detected in DNET and AG, respectively. Epigenetic mechanisms have been investigated as alternative activators of PI3K signalling in these tumours. For instance, promoter methylation and consequent silencing of expression of the gene encoding PTEN—a major negative regulator of PI3K signalling—has also been documented in some gliomas, and its frequency correlated positively with tumour grading [11, 56]. Therefore, *PTEN* promoter methylation, too, is unlikely to account for the oncogenic activation of the PI3K/AKT signalling in most grade I pLGGs.

These considerations heightened our interest in the marked down-regulation of miR-139-5p, which was found in all examined grade I pLGGs. This microRNA has been demonstrated to be a validated negative regulator of the *PIK3CA* gene, which encodes the catalytic subunit of the PI3K [38]. The oncosuppressive effects of miR-139-5p have been described in a variety of solid tumours [37, 38, 57-59], including adult high-grade gliomas [13, 14]. Nonetheless, neither the level of expression of miR-139-5p or its biological role has never been explicitly investigated in pLGGs.

Our functional characterization of miR-139-5p loss in grade I pLGGs provides the first evidence that this alteration may be a key driver of oncogenic activation of the PI3K/AKT/mTORC1 pathway in these tumours. As illustrated in *Fig. 7* the down-regulated miR-139-5p expression in supratentorial pLGGs significantly enhances activation of PI3K/AKT/mTORC1 signalling, as reflected by the high phosphorylation levels of AKT and p70 S6K, which dropped markedly after miR-139-5p

This article is protected by copyright. All rights reserved.

Accepted Article

overexpression, and the biological outcome is a substantial increase in tumour-cell proliferation. MiR-139-5p down-regulation could conceivably act alone to activate this pathway. However, there is no reason to exclude the possibility of additive effects in the presence of the genetic and/or epigenetic mechanisms of activation discussed above. It is also important to recall that miR-139-5p down-regulation might produce additional tumour-promoting effects by depressing other targets, which include numerous genes with documented oncogenic effects in gliomas and in other cancers as well (e.g., FOS, HRAS, JUN, MCL1, NOTCH1, ELTD1, ZEB1 and ZEB2) [13, 14, 38, 57, 59-61].

These conclusions are based on the results of studies on the restored expression of miR-139-5p in primary cultures of patient-derived supratentorial pLGG cells, whereas the few functional studies conducted in this area have utilized immortalized pLGG cells, such as the PA-derived Res186 line and/or Res259 cells, originally derived from a grade II diffuse astrocytoma [12, 62-64]. A major drawback of these cell lines is that they harbour genetic alterations that are relatively rare in pLGGs, and it is unclear to what extent they represent the primary lesions [12, 65, 66]. Previous attempts to use short-term primary cultures of patient-derived pLGGs have been hampered by markedly reduced growth secondary to Oncogene Induced Senescence (OIS) [8-10]. Protocol differences might contribute to explain why our efforts were more successful. It is worth noting, however, that the unsuccessful attempts cited above all involved the use of cells isolated from PAs, whereas the cells we used came from non-PA pLGGs. This choice was based on our purpose to elucidate the biology of pLGGs arising in supratentorial structures of the brain, where PAs are less common. Interestingly, however, we also encountered slow growth and senescence in our non-PA cultures (Supplementary fig. 3a-c). Senescence rates varied widely (even between cultures of cells representing the same pLGG histotype, data not shown), and they generally—but not always—increased over time. For instance, in some cultures, high rates were already observed after the first few passages. By carefully selecting the cultures destined for experiments particularly by analysing their whole genome methylation profile (Supplementary fig. 4), demonstrated to be a reliable method to pinpoint the identity of a broad range of brain tumours [10, 26, 39-41], but also continuously monitoring their senescence rates over time, we were able to complete short-term experiments and our assessment of these cells indicates that they are likely to provide reliable representations of the pLGGs seen in the clinic. Therefore our primary patient-derived pLGG cells present many benefits in comparison with the few immortalized cell lines that have been used until now and represent a more reliable model to study the biology of these tumours, that otherwise would be hardly addressed. The major disadvantage of these cultures is that they represent short-term cultures with a low proliferation rate and the number of experiments that can be performed is limited. Consequently, these primary models can be used only to answer to specific and well-defined biological questions. Interestingly, the methylation profiling allowed us to note that short-term primary cells could be more or less closer to their primary tumour, probably reflecting the heterogeneity of the cellular composition of the primary pLGG tumours analysed.

Since morbidity and mortality, particularly due to disease progression, represent a significant problem in children affected by pLGGs even after many years from diagnosis [5, 6, 67] there is an urgent need for the identification and use of less toxic therapies, such as molecular targeted agents, in children with LGGs [67]. In this context, our primary patients'-derived cellular models represent a proper and trustable *in-vitro* model to test molecular targeted compounds.

This article is protected by copyright. All rights reserved.

Accepted Article

In summary, the identification of miR-139-5p as a major regulator of the PI3K/AKT/mTORC1 axis in supratentorial pLGGs and the establishment of patients'-derived cellular models represent an important advancement and will open new perspectives to deepen the current knowledge on pLGGs biology.

Acknowledgments

The work was partially supported by Italian Ministry for Instruction, University and Research (To E. Ferretti), University La Sapienza Research Grants (To E. Ferretti), Italian Ministry of Health (To F. Locatelli), Ricerca corrente Bambino Gesù Children's Hospital (To E. Miele), Associazione EAL Onlus (To A. Mastronuzzi). We thank the Associazione Italiana per la Ricerca dei Tumori Cerebrali del Bambino (ARTUCEBA) of which S. Mascelli and A. Raso are fellows. We would like to thanks L. Moi for the technical support and M. Everett Kent for providing writing support.

Author contributions

G.C., E.F., E.M., A.P. conceived and designed research; G.C., Z.M.B., M.C., M.A., M.B., D.S., D.S., D.C. performed research; E.F., M.T., A.v.D., F.G., A.M., F.L. contributed reagents/analytic tools; G.C., Z.M.B., A.P., A.C., C.E.M., A.R., S.M. acquired and analysed data; G.C. and E.F. drafted the manuscript; all co-authors contributed to the final version of the manuscript.

Ethical approval

"All procedures performed in studies involving human participants were in accordance with the ethical standards of the institutional and/or national research committee and with the 1964 Helsinki declaration and its later amendments or comparable ethical standards."

Informed consent

"Informed consent was obtained from all individual participants for whom identifying information is included in this article and that the manuscript does not contain any directly identifiable data."

Conflict of Interest: The authors declare that they have no conflict of interest.

This article is protected by copyright. All rights reserved.

Accepted Article

References

1 Louis DN, Perry A, Reifenberger G, Von Deimling A, Figarella-Branger D, Cavenee WK, Ohgaki H, Wiestler OD, Kleihues P, Ellison DW. The 2016 World Health Organization classification of tumors of the central nervous system: a summary. Acta neuropathologica 2016; 131: 803-20

2 Pfister S, Witt O. Pediatric Gliomas. In Gliomas Ed. A von Deimling. Berlin, Heidelberg: Springer Berlin Heidelberg. 2009: 67-81

3 Project SJCsRHWUPCG. Whole-genome sequencing identifies genetic alterations in pediatric low-grade gliomas. Nature genetics 2013; 45: 602-12

4 Packer RJ, Pfister S, Bouffet E, Avery R, Bandopadhayay P, Bornhorst M, Bowers DC, Ellison D, Fangusaro J, Foreman N. Pediatric low-grade gliomas: implications of the biologic era. Neuro-oncology 2016; 19: 750-61

5 Garcia MA, Solomon DA, Haas-Kogan DA. Exploiting molecular biology for diagnosis and targeted management of pediatric low-grade gliomas. Future Oncology 2016; 12: 1493-506

6 Sturm D, Pfister SM, Jones DT. Pediatric gliomas: Current concepts on diagnosis, biology, and clinical management. Journal of Clinical Oncology 2017: JCO. 2017.73. 0242

7 Qaddoumi I, Orisme W, Wen J, Santiago T, Gupta K, Dalton JD, Tang B, Haupfear K, Punchihewa C, Easton J. Genetic alterations in uncommon low-grade neuroepithelial tumors: BRAF, FGFR1, and MYB mutations occur at high frequency and align with morphology. Acta neuropathologica 2016; 131: 833-45

8 Jacob K, Quang-Khuong D-A, Jones DT, Witt H, Lambert S, Albrecht S, Witt O, Vezina C, Shirinian M, Faury D. Genetic aberrations leading to MAPK pathway activation mediate oncogene-induced senescence in sporadic pilocytic astrocytomas. Clinical Cancer Research 2011; 17: 4650-60

9 Raabe EH, Lim KS, Kim JM, Meeker A, Mao X-g, Nikkhah G, Maciaczyk J, Kahlert U, Jain D, Bar E. BRAF activation induces transformation and then senescence in human neural stem cells: a pilocytic astrocytoma model. Clinical Cancer Research 2011; 17: 3590-9

10 Selt F, Hohloch J, Hielscher T, Sahm F, Capper D, Korshunov A, Usta D, Brabetz S, Ridinger J, Ecker J. Establishment and application of a novel patient-derived KIAA1549: BRAF-driven pediatric pilocytic astrocytoma model for preclinical drug testing. Oncotarget 2017; 8: 11460

11 Mueller S, Phillips J, Onar-Thomas A, Romero E, Zheng S, Wiencke JK, McBride SM, Cowdrey C, Prados MD, Weiss WA. PTEN promoter methylation and activation of the PI3K/Akt/mTOR pathway in pediatric gliomas and influence on clinical outcome. Neuro-oncology 2012; 14: 1146-52

12 Hütt-Cabezas M, Karajannis MA, Zagzag D, Shah S, Horkayne-Szakaly I, Rushing EJ, Cameron JD, Jain D, Eberhart CG, Raabe EH. Activation of mTORC1/mTORC2 signaling in pediatric low-grade glioma and pilocytic astrocytoma reveals mTOR as a therapeutic target. Neuro-oncology 2013; 15: 1604-14

This article is protected by copyright. All rights reserved.

Accepted Article

13 Dai S, Wang X, Li X, Cao Y. MicroRNA-139-5p acts as a tumor suppressor by targeting ELTD1 and regulating cell cycle in glioblastoma multiforme. Biochemical and biophysical research communications 2015; 467: 204-10

14 Yue S, Wang L, Zhang H, Min Y, Lou Y, Sun H, Jiang Y, Zhang W, Liang A, Guo Y. miR-139-5p suppresses cancer cell migration and invasion through targeting ZEB1 and ZEB2 in GBM. Tumor Biology 2015; 36: 6741-9

15 Miele E, Buttarelli FR, Arcella A, Begalli F, Garg N, Silvano M, Po A, Baldi C, Carissimo G, Antonelli M. High-throughput microRNA profiling of pediatric high-grade gliomas. Neuro-oncology 2013; 16: 228-40

16 Tian Y, Rich BE, Vena N, Craig JM, MacConaill LE, Rajaram V, Goldman S, Taha H, Mahmoud M, Ozek M. Detection of KIAA1549-BRAF fusion transcripts in formalin-fixed paraffin-embedded pediatric low-grade gliomas. The Journal of Molecular Diagnostics 2011; 13: 669-77

17 Jones DT, Kocialkowski S, Liu L, Pearson DM, Bäcklund LM, Ichimura K, Collins VP. Tandem duplication producing a novel oncogenic BRAF fusion gene defines the majority of pilocytic astrocytomas. Cancer research 2008; 68: 8673-7

18 Diniz MG, Gomes CC, Guimarães BVA, Castro WH, Lacerda JCT, Cardoso SV, de Faria PR, Dias FL, Eisenberg ALA, Loyola AM. Assessment of BRAFV600E and SMOF412E mutations in epithelial odontogenic tumours. Tumor Biology 2015; 36: 5649-53

19 Griffiths-Jones S, Saini HK, van Dongen S, Enright AJ. miRBase: tools for microRNA genomics. Nucleic acids research 2007; 36: D154-D8

20 Chou C-H, Chang N-W, Shrestha S, Hsu S-D, Lin Y-L, Lee W-H, Yang C-D, Hong H-C, Wei T-Y, Tu S-J. miRTarBase 2016: updates to the experimentally validated miRNA-target interactions database. Nucleic acids research 2015; 44: D239-D47

21 Suzuki R, Shimodaira H. Pvclust: an R package for assessing the uncertainty in hierarchical clustering. Bioinformatics 2006; 22: 1540-2

22 Vlachos IS, Zagganas K, Paraskevopoulou MD, Georgakilas G, Karagkouni D, Vergoulis T, Dalamagas T, Hatzigeorgiou AG. DIANA-miRPath v3. 0: deciphering microRNA function with experimental support. Nucleic acids research 2015; 43: W460-W6

23 Louis DN, Ohgaki H, Wiestler OD, Cavenee WK, Burger PC, Jouvet A, Scheithauer BW, Kleihues P. The 2007 WHO classification of tumours of the central nervous system. Acta neuropathologica 2007; 114: 97-109

24 Suh Y-L. Dysembryoplastic neuroepithelial tumors. Journal of pathology and translational medicine 2015; 49: 438

25 Luyken C, Blümcke I, Fimmers R, Urbach H, Wiestler OD, Schramm J. Supratentorial gangliogliomas: Histopathologic grading and tumor recurrence in 184 patients with a median follow□up of 8 years. Cancer 2004; 101: 146-55

This article is protected by copyright. All rights reserved.

Accepted Article

26 Sturm D, Orr BA, Toprak UH, Hovestadt V, Jones DT, Capper D, Sill M, Buchhalter I, Northcott PA, Leis I. New brain tumor entities emerge from molecular classification of CNS-PNETs. Cell 2016; 164: 1060-72

27 Ronci M, Catanzaro G, Pieroni L, Po A, Besharat ZM, Greco V, Levi Mortera S, Screpanti I, Ferretti E, Urbani A. Proteomic analysis of human sonic hedgehog (SHH) medulloblastoma stem-like cells. Mol Biosyst 2015 May 19; 11: 1603-11

28 Debacq-Chainiaux F, Erusalimsky JD, Campisi J, Toussaint O. Protocols to detect senescence-associated beta-galactosidase (SA-βgal) activity, a biomarker of senescent cells in culture and in vivo. Nature protocols 2009; 4: 1798-806

29 Po A, Silvano M, Miele E, Capalbo C, Eramo A, Salvat iV, Todaro M, Besharat Z, Catanzaro G, Cucchi D, Coni S, Di Marcotullio L, Canettieri G, Vacca A, Stassi G, De Smaele E, Tartaglia M, Screpanti I, De Maria R, Ferretti E. Noncanonical GLI1 signalling promotes stemness features and in-vivo growth in lung adenocarcinoma Oncogene 2017:

30 Ho C-Y, Bar E, Giannini C, Marchionni L, Karajannis MA, Zagzag D, Gutmann DH, Eberhart CG, Rodriguez FJ. MicroRNA profiling in pediatric pilocytic astrocytoma reveals biologically relevant targets, including PBX3, NFIB, and METAP2. Neuro-oncology 2012; 15: 69-82

31 Liu F, Xiong Y, Zhao Y, Tao L, Zhang Z, Zhang H, Liu Y, Feng G, Li B, He L. Identification of aberrant microRNA expression pattern in pediatric gliomas by microarray. Diagnostic pathology 2013; 8: 158

32 Ames HM, Yuan M, Vizcaíno MA, Yu W, Rodriguez FJ. MicroRNA profiling of low-grade glial and glioneuronal tumors shows an independent role for cluster 14q32. 31 member miR-487b. Modern Pathology 2017; 30: 204-16

33 Bao W, Fu HJ, Xie QS, Wang L, Zhang R, Guo ZY, Zhao J, Meng YL, Ren XL, Wang T. HER2 interacts with CD44 to up-regulate CXCR4 via epigenetic silencing of microRNA-139 in gastric cancer cells. Gastroenterology 2011; 141: 2076-87. e6

34 Guo H, Hu X, Ge S, Qian G, Zhang J. Regulation of RAP1B by miR-139 suppresses human colorectal carcinoma cell proliferation. The international journal of biochemistry & cell biology 2012; 44: 1465-72

35 Wong CCL, Wong CM, Tung EKK, Au SLK, Lee JMF, Poon RTP, Man K, Ng IOL. The microRNA miR-139 suppresses metastasis and progression of hepatocellular carcinoma by down-regulating Rho-kinase 2. Gastroenterology 2011; 140: 322-31

36 Mao R, Zou F, Yang L, Lin S, Li Y, Ma M, Yin P, Liang X, Liu J. The loss of MiR-139-5p promotes colitis-associated tumorigenesis by mediating PI3K/AKT/Wnt signaling. The international journal of biochemistry & cell biology 2015; 69: 153-61

37 Qiu G, Lin Y, Zhang H, Wu D. miR-139-5p inhibits epithelial–mesenchymal transition, migration and invasion of hepatocellular carcinoma cells by targeting ZEB1 and ZEB2. Biochemical and biophysical research communications 2015; 463: 315-21

This article is protected by copyright. All rights reserved.

Accepted Article

38 Krishnan K, Steptoe AL, Martin HC, Pattabiraman DR, Nones K, Waddell N, Mariasegaram M, Simpson PT, Lakhani SR, Vlassov A. miR-139-5p is a regulator of metastatic pathways in breast cancer. Rna 2013; 19: 1767-80

39 Lambert SR, Witt H, Hovestadt V, Zucknick M, Kool M, Pearson DM, Korshunov A, Ryzhova M, Ichimura K, Jabado N. Differential expression and methylation of brain developmental genes define location-specific subsets of pilocytic astrocytoma. Acta neuropathologica 2013; 126: 291-301

40 Hovestadt V, Remke M, Kool M, Pietsch T, Northcott PA, Fischer R, Florence M, Cavalli G, Ramaswamy V, Zapatka M. Robust molecular subgrouping and copy-number profiling of medulloblastoma from small amounts of archival tumour material using high-density DNA methylation arrays. Acta neuropathologica 2013; 125: 913

41 Sturm D, Witt H, Hovestadt V, Khuong-Quang D-A, Jones DT, Konermann C, Pfaff E, Tönjes M, Sill M, Bender S. Hotspot mutations in H3F3A and IDH1 define distinct epigenetic and biological subgroups of glioblastoma. Cancer cell 2012; 22: 425-37

42 Hayes J, Peruzzi PP, Lawler S. MicroRNAs in cancer: biomarkers, functions and therapy. Trends in molecular medicine 2014; 20: 460-9

43 Bracken CP, Scott HS, Goodall GJ. A network-biology perspective of microRNA function and dysfunction in cancer. Nature Reviews Genetics 2016; 17: 719-32

44 Braoudaki M, Lambrou G, Papadodima S, Stefanaki K, Prodromou N, Kanavakis E. MicroRNA expression profiles in pediatric dysembryoplastic neuroepithelial tumors. Medical Oncology 2016; 33: 5

45 Birks DK, Barton VN, Donson AM, Handler MH, Vibhakar R, Foreman NK. Survey of MicroRNA expression in pediatric brain tumors. Pediatric blood & cancer 2011; 56: 211-6

46 Jones TA, Jeyapalan JN, Forshew T, Tatevossian RG, Lawson AR, Patel SN, Doctor GT, Mumin MA, Picker SR, Phipps KP, Michalski A, Jacques TS, Sheer D Molecular analysis of pediatric brain tumors identifies microRNAs in pilocytic astrocytomas that target the MAPK and NF-κB pathways. Acta neuropathologica communications 2015; 3: 86

47 Laddha SV, Nayak S, Paul D, Reddy R, Sharma C, Jha P, Hariharan M, Agrawal A, Chowdhury S, Sarkar C. Genome-wide analysis reveals downregulation of miR-379/miR-656 cluster in human cancers. Biology direct 2013; 8: 10

48 Skalsky RL, Cullen BR. Reduced expression of brain-enriched microRNAs in glioblastomas permits targeted regulation of a cell death gene. PloS one 2011; 6: e24248

49 Jha P, Agrawal R, Pathak P, Kumar A, Purkait S, Mallik S, Suri V, Chand Sharma M, Gupta D, Suri A. Genome□wide small noncoding RNA profiling of pediatric high□grade gliomas reveals deregulation of several miRNAs, identifies downregulation of snoRNA cluster HBII□52 and delineates H3F3A and TP53 mutant□specific miRNAs and snoRNAs. International journal of cancer 2015; 137: 2343-53

This article is protected by copyright. All rights reserved.

Accepted Article

50 Yeh W-L, Lin H-Y, Huang C-Y, Huang B-R, Lin C, Lu D-Y, Wei K-C. Migration-prone glioma cells show curcumin resistance associated with enhanced expression of miR-21 and invasion/anti-apoptosis-related proteins. Oncotarget 2015; 6: 37770

51 Northcott PA, Fernandez-L A, Hagan JP, Ellison DW, Grajkowska W, Gillespie Y, Grundy R, Van Meter T, Rutka JT, Croce CM. The miR-17/92 polycistron is up-regulated in Sonic Hedgehog–driven medulloblastomas and induced by N-myc in Sonic Hedgehog–treated cerebellar neural precursors. Cancer research 2009; 69: 3249-55

52 Murphy BL, Obad S, Bihannic L, Ayrault O, Zindy F, Kauppinen S, Roussel MF. Silencing of the miR-17□92 cluster family inhibits medulloblastoma progression. Cancer research 2013; 73: 7068-78

53 Grunder E, D'Ambrosio R, Fiaschetti G, Abela L, Arcaro A, Zuzak T, Ohgaki H, Lv S-Q, Shalaby T, Grotzer M. MicroRNA-21 suppression impedes medulloblastoma cell migration. European journal of cancer 2011; 47: 2479-90

54 Baker SJ, Ellison DW, Gutmann DH. Pediatric gliomas as neurodevelopmental disorders. Glia 2016; 64: 879-95

55 Khatua S, Wang J, Rajaram V. Review of low-grade gliomas in children—evolving molecular era and therapeutic insights. Child's Nervous System 2015; 31: 643-52

56 Wiencke JK, Zheng S, Jelluma N, Tihan T, Vandenberg S, Tamgüney T, Baumber R, Parsons R, Lamborn KR, Berger MS. Methylation of the PTEN promoter defines low-grade gliomas and secondary glioblastoma. Neuro-oncology 2007; 9: 271-9

57 Zhang L, Dong Y, Zhu N, Tsoi H, Zhao Z, Wu CW, Wang K, Zheng S, Ng SS, Chan FK. microRNA-139-5p exerts tumor suppressor function by targeting NOTCH1 in colorectal cancer. Molecular cancer 2014; 13: 124

58 Song M, Yin Y, Zhang J, Zhang B, Bian Z, Quan C, Zhou L, Hu Y, Wang Q, Ni S. MiR-139-5p inhibits migration and invasion of colorectal cancer by downregulating AMFR and NOTCH1. Protein & cell 2014; 5: 851-61

59 Li RY, Chen LC, Zhang HY, Du WZ, Feng Y, Wang HB, Wen JQ, Liu X, Li XF, Sun Y. MiR□139 inhibits Mcl□1 expression and potentiates TMZ□induced apoptosis in glioma. CNS neuroscience & therapeutics 2013; 19: 477-83

60 Fan Q, He M, Deng X, Wu WK, Zhao L, Tang J, Wen G, Sun X, Liu Y. Derepression of c□Fos caused by MicroRNA□139 down□regulation contributes to the metastasis of human hepatocellular carcinoma. Cell biochemistry and function 2013; 31: 319-24

61 Zhang H-d, Jiang L-h, Sun D-w, Li J, Tang J-h. MiR-139-5p: promising biomarker for cancer. Tumor Biology 2015; 36: 1355-65

62 Brandt WD, Schreck KC, Bar EE, Taylor I, Marchionni L, Raabe E, Eberhart CG, Rodriguez FJ. Notch signaling activation in pediatric low-grade astrocytoma. Journal of Neuropathology & Experimental Neurology 2015; 74: 121-31

This article is protected by copyright. All rights reserved.

Accepted Article

63 Ajeawung NF, Faure R, Jones C, Kamnasaran D. Preclinical evaluation of dipotassium bisperoxo (picolinato) oxovanadate V for the treatment of pediatric low-grade gliomas. Future Oncology 2013; 9: 1215-29

64 Ajeawung NF, Maltais R, Jones C, Poirier D, Kamnasaran D. Viability screen on pediatric low grade glioma cell lines unveils a novel anti-cancer drug of the steroid biosynthesis inhibitor family. Cancer letters 2013; 330: 96-105

65 Bax DA, Little SE, Gaspar N, Perryman L, Marshall L, Viana-Pereira M, Jones TA, Williams RD, Grigoriadis A, Vassal G. Molecular and phenotypic characterisation of paediatric glioma cell lines as models for preclinical drug development. PloS one 2009; 4: e5209

66 Henriquez NV, Forshew T, Tatevossian R, Ellis M, Richard-Loendt A, Rogers H, Jacques TS, Reitboeck PG, Pearce K, Sheer D. Comparative expression analysis reveals lineage relationships between human and murine gliomas and a dominance of glial signatures during tumor propagation in vitro. Cancer research 2013; 73: 5834-44

67 Upadhyaya SA, Ghazwani Y, Wu S, Broniscer A, Boop FA, Gajjar A, Qaddoumi I. Mortality in children with low□grade glioma or glioneuronal tumors: A single□institution study. Pediatric Blood & Cancer 2017

Figure Legends

Fig. 1 Hierarchical clustering of microRNAs displaying differential expression in pLGGs vs. non-neoplastic brain tissues (CTRL). Hierarchical clustering of the 93 microRNAs differentially expressed in pLGGs vs. CTRL (grey) ($p<0.05$) was performed and the Euclidean method was used to generate clusters on the basis of delta Ct values. Tissue: PA, pilocytic astrocytoma (blue); GG, ganglioglioma (red); GNT, glioneuronal tumour (purple); DNET, dysembryoplastic neuroepithelial tumour (orange); AG, angiocentric glioma (light blue). BRAF status was defined exclusively by the presence/absence of the V600E point mutation (green) and KIAA1549-BRAF fusion variants (yellow) (KIAA1549-BRAF exon 16-exon 9, KIAA1549-BRAF exon 16-exon 11, or KIAA1549-BRAF exon 15-exon 9). NEG, negative for all analysed mutations (black)

Fig. 2 Immunofluorescence characterization of primary patient-derived pLGG cells. (a-c) Single-cell monolayers (on the average present after 7 days of culture) were subjected to immunofluorescence staining for glial markers (S100, vimentin, glial fibrillary acidic protein [GFAP]) and neuronal markers (NeuN, synaptophysin). In detail, **(a)** AG-derived cells (pLGG1) show positivity for glial markers only [23], whereas **(b)** DNET-derived cells (findings shown for pLGG2 are also representative of DNET line pLGG3) [24] and **(c)** GG-derived cells (pLGG4) expressed both glial and neuronal markers [25]. The positivity and negativity of the staining of the observed glial and neuronal markers was concordant with IHC staining results obtained by pathologists on FFPE samples of the tumours from which pLGG lines 1, 2, and 4 were derived (Data not shown). Scale bars, 50 µm and 100 µm (high magnification insert).

This article is protected by copyright. All rights reserved.

Accepted Article

Fig. 3 Methylation analysis of primary patient-derived pLGG cells confirms their identity. DNA methylation profiling was performed on the three tumours (an AG and two DNETs) that did not show any genetic BRAF alterations and their primary pLGG derived cells. TSNE (t-Distributed Stochastic Neighbor Embedding) analysis of the whole genome DNA methylation data show a close similarity between patient-derived pLGG cell lines, their primary tissues and the group of pLGGs they derive from (AG and DNET) but they diverge from other paediatric low-grade tumours and non-neoplastic cortex. pLGG1, AG tissue and patient-derived cells; pLGG2 and pLGG3, DNET tissues and their respective patient-derived cells (see Table 2). Colour legend of the TSNE plot as follows: PXA (brown); GG (orange); Cortex (light blue); AG (black); PA GG hemispheric (light purple); PA Infratentorial (purple); DNET (blue); PA midline (yellow). *Abbreviations:* AG, angiocentric glioma; DNET, dysembryoplastic neuroepithelial tumour; GG, ganglioglioma; PA, pilocytic astrocytoma; PXA, pleomorphic xanthoastrocytoma.

Fig. 4 Downregulation of miR-139-5p in pLGGs favours tumour cell-proliferation. (a-b) Single assay qPCR validation of downregulated miR-139-5p expression in **(a)** supratentorial pLGG tissues and **(b)** patient-derived primary pLGG cell lines and their corresponding tissues *versus* non-neoplastic total brain tissue (CTRL) **(c-f)** Effects on cell proliferation of miR-139-5p overexpression in cultured cells from **(c)** primary AG, **(d)** primary DNET indicated as pLGG2, **(e)** primary DNET indicated as pLGG3 and **(f)** primary GG. Cells were transfected with 20 nM miR-139-5p or an empty vector (CTRL) and subjected to trypan blue staining 48 h later. Relative cell growth refers to fold over CTRL. * $p<0.05$ *versus* CTRL

Fig. 5 PI3K/AKT signalling pathway inhibition decreases pLGG AKT phosphorylation and cell proliferation. (a-c) Phosphorylated AKT (p-AKT) and total AKT levels were measured in supratentorial primary pLGG cells transfected with miR-139-5p or empty vector (CTRL) **(d-g)** AG **(d)** pLGG2 (DNET) **(e)** pLGG3 (DNET) **(f)** and GG **(g)** cells were treated for 30 min with 50 µM LY294002 and assayed for proliferation (Trypan Blue exclusion) after a 48 h recovery period in normal medium. **(h-j)** p-AKT and total AKT levels were measured in supratentorial primary pLGG cells treated with 50 µM LY294002 for 30 min or vehicle alone (CTRL) after a 48 h recovery period in normal medium. Relative cell growth refers to fold over CTRL. * $p<0.05$, ** $p<0.001$ *versus* CTRL

Fig. 6 Phosphorylation of p70 S6K in pLGG cells subjected to miR-139-5p overexpression or LY294002 treatment. The overexpression of miR-139-5p **(a-c)** and direct PI3K inhibition for 30 min with 50 µM LY294002 followed by a 48 h recovery period in normal medium **(d-f)** both strongly reduced p70 S6K phosphorylated levels (p-p70 S6K) while leaving unaffected the level of total p70 S6K.

This article is protected by copyright. All rights reserved.

Accepted Article

Fig. 7 Downregulation of miR-139-5p expression in pLGGs promotes proliferation by de-repressing PI3K/AKT/mTORC1 signalling. miR-139-5p, that targets the 3'-UTR of *PIK3CA*, is strongly downregulated in pLGG tumours resulting in the hyper-activation of the PI3K/AKT pathway. After miR-139-5p overexpression in pLGG primary cells both AKT and p70 S6K phosphorylation levels are reduced, with a consistent significant impairment in cell proliferation. PTEN, phosphatase and tensin homolog; PI3K, phosphatydil-inositol-3-kinase; PDK-1, phosphoinositide-dependent kinase 1; TSC2, tuberous sclerosis complex 2; Rheb, Ras homolog enriched in brain; mTORC1, mammalian target of rapamycin 1; p70 S6K, p70 S6 kinase.

Supplementary Figure Legends

Supplementary Fig. 1 Hierarchical clustering of microRNAs displaying differential expression in pLGGs vs. pHGGs Hierarchical clustering of the 60 microRNAs differentially expressed in pLGGs vs. pHGGs. The Euclidean method was used to generate clusters based on delta Ct values. Tissue: PA, pilocytic astrocytoma (blue); GG, ganglioglioma (red); GNT, glioneuronal tumour (purple); DNET, dysembryoplastic neuroepithelial tumour (orange); AG, angiocentric glioma (light blue); pHGG, paediatric high-grade gliomas (brown)

Supplementary Fig. 2 Expression of PIK3CA in pLGG tissues. (a) *Top:* Representative images of immunohistochemical (IHC) staining for PIK3CA in AG, DNET and GG show positive staining in cytoplasm of neoplastic cells. *Bottom:* Negative control performed omitting primary antibody. **(b)** *Left:* Representative images of hepatocellular carcinoma sample used as positive control used for PI3KA imuunohistochemical assay. *Right:* Negative control was performed omitting primary antibody. Scale bars: 20 μm. Original magnification ×20.

Supplementary Fig. 3 Expression of the senescence marker SA-β-gal in patient-derived primary pLGG cells. Representative images of SA-β-gal expression in two of the primary cell cultures used in the study: **(a)** pLGG4 cells derived from a GG and **(b)** pLGG2 cells from a DNET. Both displayed low SA-β-gal-positivity rates (less than 20%). In contrast, in panel **(c)** a representative image of pLGG4 at passage 12 is reported. The very low proliferation rate and high percentage of SA-β-gal-positive cells reached by these cells rendered them unsuitable for further biological investigations. Scale bar, 100 μm. **(d)** Growth curves of patient-derived primary pLGG cells from T0 until passage 8 (ps8); pLGG1 cells derived from an AG (blue), pLGG2 cells from a DNET (green) and pLGG4 cells derived from a GG (orange).

This article is protected by copyright. All rights reserved.

Accepted Article

Supplementary Fig. 4 Methylation profile and copy number variation (CNV) of primary patients' derived pLGG cells shows a close similarity to the primary tumour. (a) Unsupervised hierarchical clustering of the whole genome DNA methylation data performed by using Illumina GenomeStudio V2011.1 showed a close similarity between the primary tumours and their corresponding cells. This result indicates that the innate methylation profile of the cell of origin was unaffected from the process of *in vitro* culture. **(b)** CNV analysis shows chromosome 1 to 22 (and X/Y if automatic prediction was successful). Gains/amplifications represent positive - green, losses negative-red deviations from the baseline. 29 brain tumour relevant gene regions are highlighted for easier assessment. (see, http://www.bioconductor.org/packages/devel/bioc/html/conumee.html). A specific genetic alteration is highlightened (red arrow) when present.

pLGG1 primary cells derive from an AG tumour (see Table 2), pLGG2 and pLGG3 primary cells derive from two DNET tumours (see Table 2). *Abbreviations:* AG, angiocentric glioma; DNET, dysembryoplastic neuroepithelial tumour

Supplementary Fig. 5 Levels of miR-139-5p before and after its overexpression in the four primary pLGG cell lines (derived from an AG, two DNETs, and a GG). Cells were transfected with 20 nM miR-139-5p and assayed 48 h later. **(a)** MiR-139-5p level in non-neoplastic brain tissues (CTRL) was 68-fold higher than that found in the pLGG cells at baseline. **(b-d)** Post-transfection assays of **(b)** AG cells, **(c)** DNET cells, and **(d)** GG cells revealed mean miR-139-5p levels approximately 30-fold higher than those found at baseline (CTRL). * $p<0.05$, *** $p<0.001$ *versus* indicated CTRL

Supplementary Fig. 6 Expression of p-p70 S6K in pLGG tissues. **(a)** *Top:* Representative images of cytoplasmic immunostaining for phospho-p70 S6 kinase (p-p70 S6K) in AG, DNET and GG samples. *Bottom:* Negative control was performed omitting primary antibody. **(b)** *Left:* Human breast cancer was used as positive control for p-p70 S6K staining. *Right:* Negative control was performed omitting primary antibody. Scale bars: 20 μm. Original magnification ×20.

Supplementary Fig. 7 Expression of p-AKT in pLGG tissues. **(a)** *Top:* Representative images of supratentorial pLGG samples showing positive staining for phospho-AKT (p-AKT). *Bottom:* Negative control was performed omitting primary antibody. **(b)** *Left:* Human breast cancer was used as positive control to detect p-AKT immunopositivity. *Right:* Negative control was performed omitting primary antibody. Scale bars: 20 μm. Original magnification ×20.

This article is protected by copyright. All rights reserved.

Accepted Article

Table 1. Clinical-pathological features of the 45 pLGG cases subjected to microRNA expression profiling

Sample	Age at diagnosis (y)	Sex	Histology	WHO grade	Location	BRAF alterations[a]
P5	3	M	AG	II	Supra	--
P38[b]	12.3	M	AG	I	Supra	--
P3[b]	9	F	DNET	I	Supra	--
P11	10	F	DNET	I	Supra	--
P16[b]	5.8	M	DNET	I	Supra	--
P32	8.4	F	DNET	I	Supra	--
P8	7.6	F	GG	I	Supra	--
P18[b]	14.7	F	GG	I	Supra	V600E
P19	4.5	M	GG	I	Infra	V600E
P22	8	F	GG	I	Infra	K16B9
P26	7	F	GG	I	Supra	--
P29	11.3	M	GG	I	Infra	--
P36	5.5	M	GG	I	Infra	K15B9
P41	1.6	M	GG	I	BS	--
P33	9.1	F	GNT	I	Infra	K15B9
P1	15	F	PA	I	Infra	--
P2	1	F	PA	I	Infra	K16B9
P4	12	M	PA	I	Infra	--
P6	9	M	PA	I	Supra	K16B9
P7	6.1	F	PA	I	Infra	K16B9
P9	1.9	F	PA	I	Infra	K15B9
P10	16.2	M	PA	I	Infra	--
P12	3.8	M	PA	I	Infra	K16B9
P13	5.7	M	PA	I	Infra	--
P14	1.3	F	PA	I	Infra	--
P15	10	F	PA	I	Infra	--
P17	12	M	PA	I	Infra	--
P20	4.4	F	PA	I	Infra	K16B9
P21	10	M	PA	I	Supra	--
P23	11	F	PA	I	Infra	--
P24	3	M	PA	I	Supra	K16B9
P25	9.4	F	PA	I	BS	K16B9
P27	10	M	PA	I	Infra	K16B9
P28	7	F	PA	I	BS	--
P30	6.8	F	PA	I	Supra	K16B11
P31	10.2	M	PA	I	Infra	K16B9
P34	5	M	PA	I	Supra	--
P35	7.5	M	PA	I	Infra	K16B9
P37	3.2	M	PA	I	Supra	K15B9
P39	6.6	M	PA	I	Supra	--
P40	1.4	M	PA	I	Infra	K16B9
P42	3.3	M	PA	I	Infra	--
P43	1.8	F	PA	I	Infra	--

This article is protected by copyright. All rights reserved.

Accepted Article

P44	3.6	M	PA	I	Supra	K15B9
P45	3.1	M	PA	I	Infra	V600E

Abbreviations: AG, angiocentric glioma; BS, brain stem; DNET, disembryoplastic neuroepithelial tumour; GG, ganglioglioma; GNT, glioneruonal tumor; Infra, infratentorial; PA, pilocytic astrocytoma; pLGG, pediatric low-grade glioma; Supra, supratentorial; --, Not detected.

[a] BRAF screening was limited to the V600E point mutation and three gene fusions (KIAA1549-BRAF exon 16-exon 9 [K16B9], KIAA1549-BRAF exon 16-exon 11 [K16B11], KIAA1549-BRAF exon 15-exon 9 [K15B9]).

[b] Primary pLGG cell lines were derived from these tumors (see Table 2)

Table 2. Clinical-pathological features of patient-derived primary pLGG cell lines

Sample	Parental Tumor	Age at diagnosis	Sex	Histology	Location	BRAF alterations[a]	
						Tumor tissue	Isolated cells
pLGG1	P38	12.3	M	AG	Supra	--	--
pLGG2	P3	9	F	DNET	Supra	--	--
pLGG3	P16	5.8	M	DNET	Supra	--	--
pLGG4	P18	14.7	F	GG	Supra	V600E	V600E

Abbreviations: AG, angiocentric glioma; DNET, disembryoplastic neuroepithelial tumour; GG, ganglioglioma; NS, not screened; pLGG, pediatric low-grade glioma; Supra, supratentorial; --, Not detected.

[a] BRAF screening was limited to the V600E point mutation and three gene fusions (KIAA1549-BRAF exon 16-exon 9 [K16B9], KIAA1549-BRAF exon 16-exon 11 [K16B11], KIAA1549-BRAF exon 15-exon 9 [K15B9]).

This article is protected by copyright. All rights reserved.

Accepted Article

Table 3. MicroRNAs displaying significantly upregulated expression in supratentorial pLGGs with respect to non-neoplastic brain tissues (CTRL).

microRNA	LFC	P-value	Part of cluster	Chr
hsa-miR-663b	46.20	3.99E-03		
hsa-miR-193a-3p	45.40	4.06E-02		
hsa-miR-378	31.89	1.60E-02		
hsa-miR-576-3p	17.65	2.46E-02		
hsa-miR-1275	17.02	2.57E-02		
hsa-miR-1225-3p	15.70	1.84E-02		
hsa-miR-337-5p	11.84	4.34E-02	493~136	chr14
hsa-miR-550a-3p	11.32	2.16E-03	550a~550b	chr7
hsa-miR-483-5p	10.93	1.05E-02		
hsa-miR-18a-5p	10.34	1.20E-02	17~92a-1	chr13
hsa-miR-720	9.61	3.38E-04		
hsa-miR-1233-3p	9.47	2.63E-02		
hsa-miR-106b-3p	6.43	3.29E-03	106b~25	chr7
hsa-miR-296-5p	6.05	4.68E-03	298~296	chr20
hsa-miR-29a-5p	5.96	4.09E-02	29b-1~29a	chr7
hsa-miR-661	5.95	9.16E-03		
hsa-miR-9-3p	5.53	9.78E-04		
hsa-miR-1260a	5.21	5.65E-04		
hsa-miR-301a-3p	5.15	8.52E-04		
hsa-miR-497-5p	4.69	9.94E-05	497~195	chr17
hsa-miR-99a-3p	3.88	3.27E-03	99a~let-7c	chr21
hsa-miR-455-5p	3.85	2.14E-02		
hsa-miR-34a-3p	3.42	2.33E-02		
hsa-miR-27a-3p	2.97	1.98E-02	23a~24-2	chr19
hsa-miR-19a-3p	2.81	0.042344329	17~92a-1	chr13
hsa-miR-362-5p	2.34	3.19E-02	532~502	chrX
hsa-miR-193a-5p	2.32	4.57E-02		
hsa-miR-181a-2-3p	2.14	3.68E-02	181a-2~181b-2	chr9

Abbreviations: LFC, Linear Fold Change; Chr, Chromosome

This article is protected by copyright. All rights reserved.

Accepted Article

Table 4. MicroRNAs displaying significantly downregulated expression in supratentorial pLGGs with respect to non-neoplastic brain tissues (CTRL).

microRNA	LFC	P-value	Part of cluster	Chr
hsa-miR-147b	0.006	7.85E-03		
hsa-miR-512-3p	0.007	1.93E-02	512-1~519a-2	chr19
hsa-miR-657	0.009	4.90E-02	1250~657	chr17
hsa-miR-523-3p	0.016	4.90E-02	512-1~519a-2	chr19
hsa-miR-485-5p	0.017	2.82E-03	379~656	chr14
hsa-miR-138-2-3p	0.017	8.82E-03		
hsa-miR-187-3p	0.024	2.58E-02		
hsa-miR-522-3p	0.044	3.44E-02	512-1~519a-2	chr19
hsa-miR-425-3p	0.044	1.17E-02	191~425	chr3
hsa-miR-423-5p	0.048	3.08E-03	423~3184	chr17
hsa-miR-577	0.083	2.72E-02		
hsa-miR-889-3p	0.100	4.60E-02	379~656	chr14
hsa-miR-184	0.108	3.24E-02		
hsa-miR-128-3p	0.114	2.69E-02		
hsa-miR-133a-3p	0.144	9.51E-03	1-2~133a-1	chr18
hsa-miR-139-5p	0.147	3.68E-02		
hsa-miR-203a	0.153	2.05E-02	203a~203b	chr14
hsa-miR-31-5p	0.156	3.28E-02		
hsa-miR-23b-3p	0.168	4.04E-02	23b~24-1	chr9
hsa-miR-654-5p	0.172	2.18E-02		
hsa-miR-495-3p	0.184	1.07E-02	379~656	chr14
hsa-miR-539-5p	0.198	5.34E-03	379~656	chr14
hsa-miR-149-5p	0.200	3.98E-02		
hsa-miR-138-5p	0.205	2.60E-02		
hsa-miR-7-1-3p	0.215	3.27E-02		
hsa-miR-487b-3p	0.215	1.56E-02	379~656	chr14
hsa-miR-625-5p	0.226	3.35E-02		
hsa-miR-132-3p	0.252	1.18E-02	212~132	chr17
hsa-miR-330-3p	0.266	0.011063144		
hsa-miR-628-5p	0.270	8.66E-03		
hsa-miR-323a-3p	0.270	3.29E-02	379~656	chr14
hsa-miR-410-3p	0.276	2.29E-02	379~656	chr14
hsa-miR-491-5p	0.277	7.67E-03		
hsa-miR-95-3p	0.332	3.67E-02		
hsa-miR-379-5p	0.345	1.59E-02	379~656	chr14
hsa-miR-342-3p	0.350	2.66E-02	342~151b	chr14
hsa-miR-200c-3p	0.362	3.55E-02	200c-141	chr12
hsa-miR-411-5p	0.412	0.024012639	379~656	chr14
hsa-miR-126-3p	0.418	3.91E-02		
hsa-miR-103a-3p	0.450	3.53E-02		
hsa-miR-191-5p	0.493	3.44E-02	191~425	chr3

Abbreviations: LFC, Linear Fold Change; Chr, Chromosome

This article is protected by copyright. All rights reserved.

Accepted Article

Table 5. The 20 most markedly enriched biological processes using up- or down-regulated microRNAs in pLGGs. Processes were identified and ranked according to p-value, as assigned in KEGG pathway analysis using DIANA-miRPath (v. 3.0).

	KEGG pathway	p-value	#genes	#microRNAs
Up regulated microRNAs in pLGG vs CTRLs	Proteoglycans in cancer	3.31E-10	144	62
	Signaling pathways regulating pluripotency of stem cells	1.19E-07	104	65
	Pathways in cancer	8.43E-06	263	63
	Wnt signaling pathway	1.68E-05	100	61
	Rap1 signaling pathway	1.50E-04	144	63
	Ras signaling pathway	3.51E-04	151	62
	PI3K-Akt signaling pathway	4.91E-04	223	66
	Focal adhesion	4.91E-04	141	64
	Regulation of actin cytoskeleton	3.10E-03	142	62
	MAPK signaling pathway	9.55E-03	163	62
Down regulated microRNAs in pLGG vs CTRLs	Hippo signaling pathway	3.78E-09	114	53
	Pathways in cancer	5.31E-08	278	58
	Axon guidance	1.77E-07	100	53
	Proteoglycans in cancer	1.82E-07	142	55
	Rap1 signaling pathway	6.52E-05	148	53
	PI3K-Akt signaling pathway	6.29E-04	226	53
	Oxytocin signaling pathway	1.98E-03	109	53
	Ras signaling pathway	1.68E-02	146	54
	Regulation of actin cytoskeleton	1.97E-02	141	54
	HTLV-I infection	3.07E-02	167	55

This article is protected by copyright. All rights reserved.

Accepted Article

Fig. 1

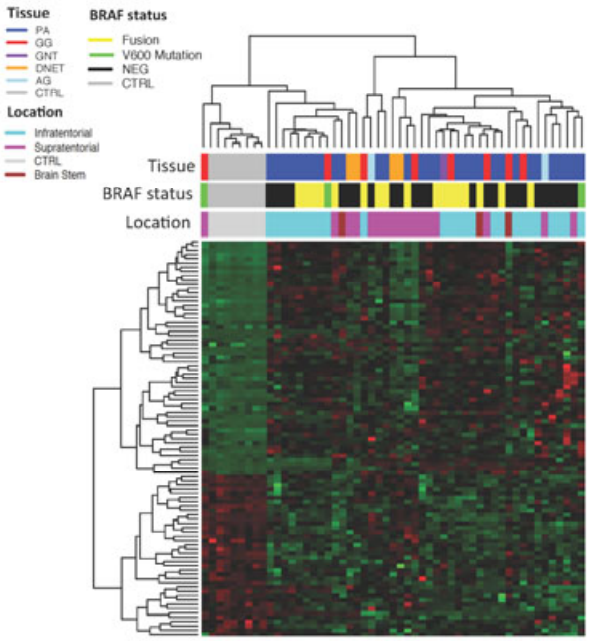

This article is protected by copyright. All rights reserved.

Accepted Article

Fig. 2

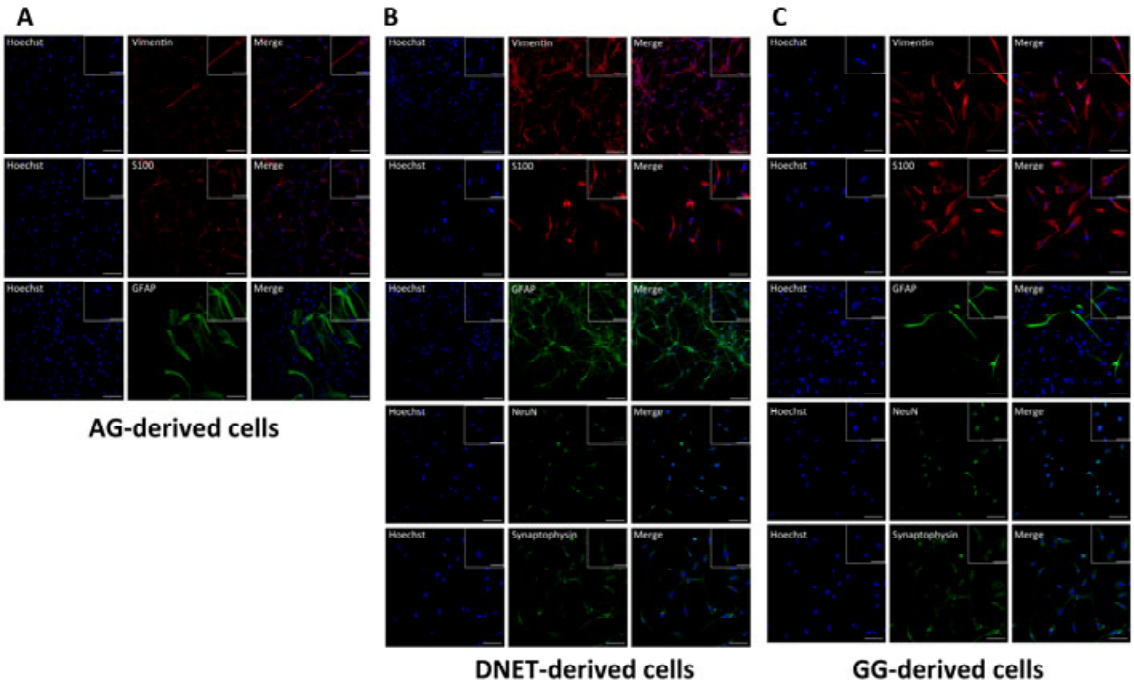

This article is protected by copyright. All rights reserved.

Accepted Article

Fig. 3

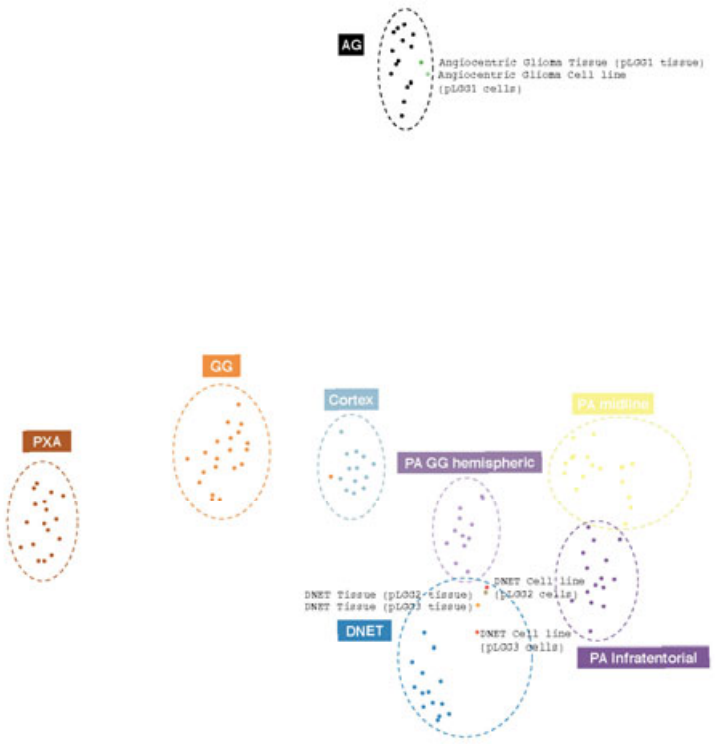

This article is protected by copyright. All rights reserved.

Accepted Article

Fig. 4

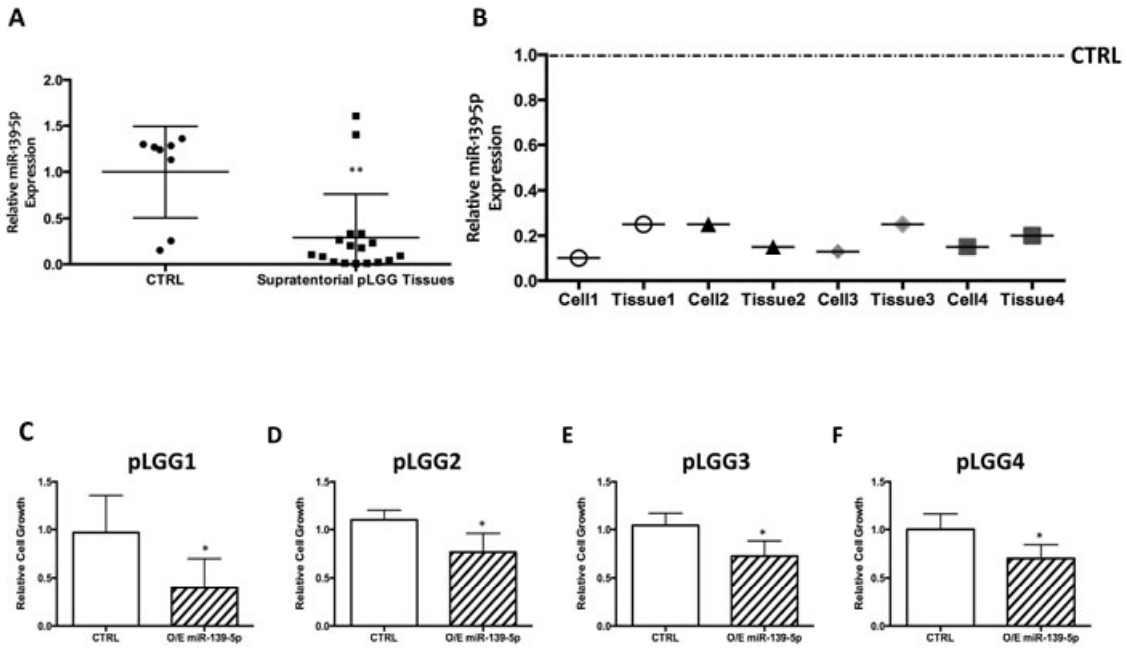

This article is protected by copyright. All rights reserved.

Accepted Article

Fig. 5

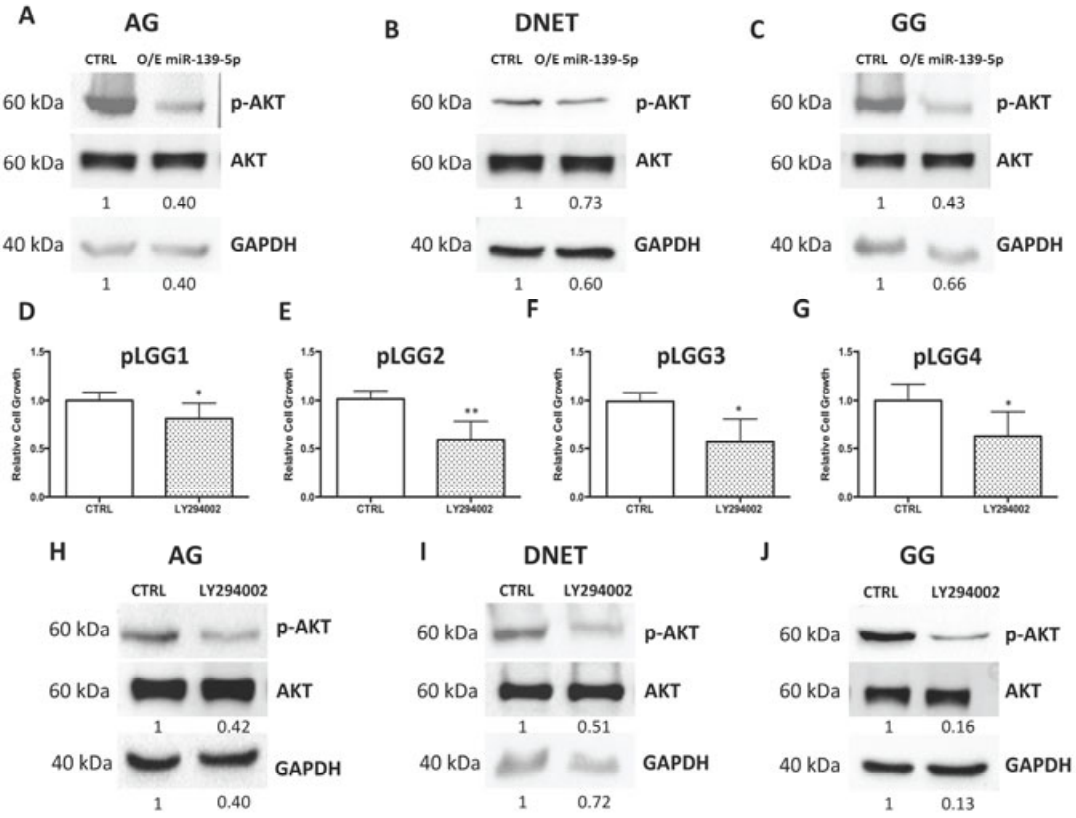

This article is protected by copyright. All rights reserved.

Accepted Article

Fig. 6

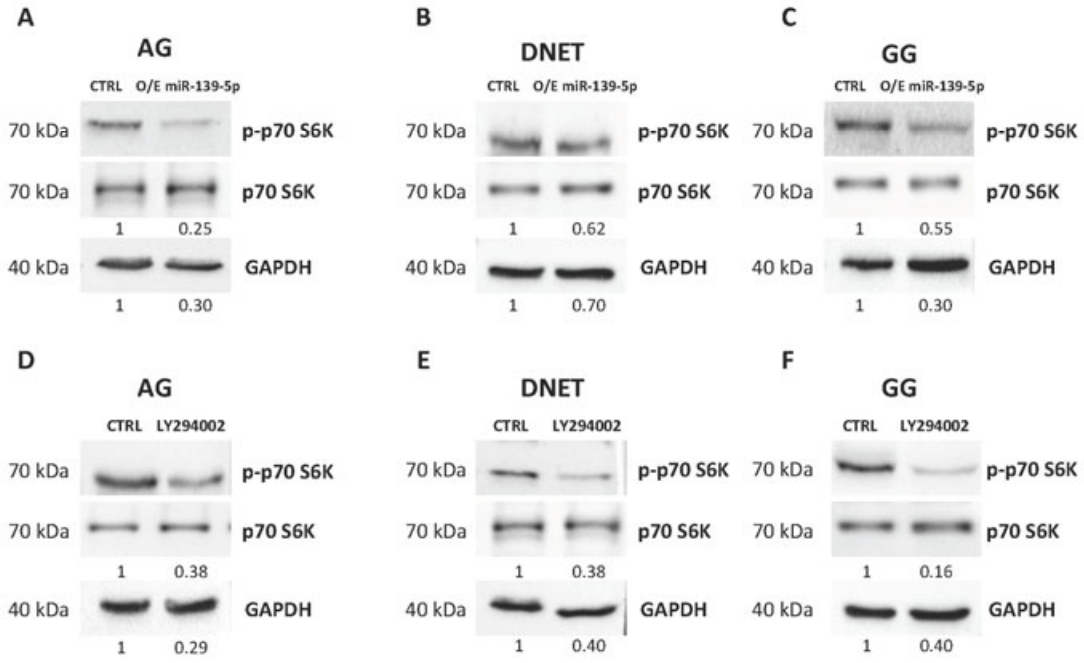

This article is protected by copyright. All rights reserved.

Accepted Article

Fig. 7

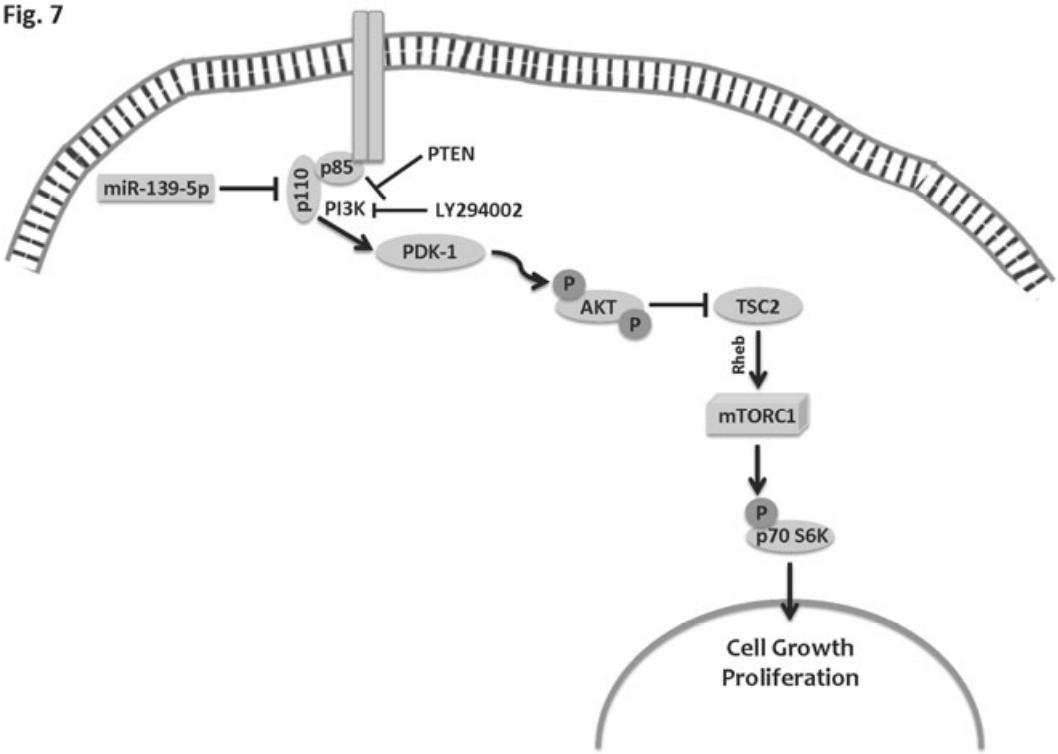

This article is protected by copyright. All rights reserved.